Check for updates

Journal of Hydrogen and New Energy, Vol. 34, No. 5, 2023, pp. 497~504
DOI: https://doi.org/10.7316/JHNE.2023.34.5.497

JHNE
pISSN 1738-7264 • eISSN 2288-7407

수소 충전 시스템용 리셉터클의 내부 압력 분포와 압력 강하에 관한 수치적 연구

왕위엔강[1] · 이승혁[1] · 손채훈[1†] · 이세동[2] · 이현복[2]

[1]세종대학교 기계공학과, [2]LT정밀(주)

A Numerical Analysis of Pressure Distribution and Pressure Drop in Receptacle for Hydrogen Charging System

YUANGANG WANG[1], SEUNGHYEOK LEE[1], CHAE HOON SOHN[1†], SEDONG LEE[2], HYUNBOK LEE[2]

[1]Department of Mechanical Engineering, Sejong University, 209 Neungdong-ro, Gwangjin-gu, Seoul 05006, Korea
[2]LT Precision, 67 Changwon-daero 1144beon-gil, Seongsan-gu, Changwon 51540, Korea

[†]Corresponding author : chsohn@sejong.ac.kr

Received 26 June, 2023
Revised 28 August, 2023
Accepted 12 October, 2023

Abstract >> This study analyzes pressure distribution and pressure drop in the receptacle used in charging system of hydrogen fuel cell vehicles. The objective is to minimize receptacle-induced pressure drop by redesigning internal flow channels. Through numerical simulations, three receptacle variants are compared with a baseline case. Results show reduced pressure drop in the filter section. However, the check valve section exhibits higher pressure drop, requiring further improvement. By increasing throat diameter, pressure drop is decreased by 28% between inlet and outlet of the receptacle. This study shows the relationship between dynamic pressure and pressure drop, providing a guideline for receptacle performance optimization. The redesigned receptacle offers potential for enhancing hydrogen charging efficiency.

Key words : Receptacle(리셉터클), Pressure distribution(압력 분포), Pressure drop (차압), Filter(필터), Check valve(체크밸브)

1. Introduction

Rising global concerns over the emissions of pollutants from classical internal combustion engines have prompted implementation of stricter exhaust emission regulations[1,2]. As a result, there has been a growing demand for environment-friendly vehicles to replace conventional internal combustion engine vehicles. Hydrogen fuel cell electric vehicles (FCEVs) have emerged as a promising alternative by utilizing hydrogen as a clean energy source. The purity and cleanliness of the hydrogen fuel are essential to maintain the optimal performance and longevity of fuel cell systems in FCEVs[3,4]. International standards and

regulations have been established to address this issue to govern the quality of hydrogen gas used in refueling systems[5]. Various purification and filtration technologies, including receptacles equipped with filters, are employed to remove or reduce these impurities and ensure the delivery of high-quality hydrogen fuel to FCEVs. Consequently, extensive study has focused on improving receptacle performance by optimizing refueling efficiency.

The receptacle plays a crucial role as a critical component in hydrogen refueling systems. Its internal configuration significantly influences fluid behavior during refueling. Ye et al[6,7]. investigated the effect of the spool-head angle and shape of receptacles on the movement performance of the valve spool and flow field characteristics. The structural optimization of the check valve was conducted by them. To minimize the vibration and noise induced by the receptacle, Lee et al[8]. employed two different valve models and conducted numerical analyses under varying flow conditions. They successfully demonstrated that alterations in the channel shape led to reduced vibration and noise levels. Choi et al[9]. studied the internal flow of the receptacle and found that reducing the diameter of the poppet is advantageous for improving performance. These studies collectively establish significant influence of internal variations on the performance of the receptacle.

In this study, the objective is to investigate the pressure drop caused by the receptacle. The research aimed to reduce the pressure drop by analyzing the pressure distribution within the internal flow channel. A comparison is made between the re-designed variants and the baseline receptacle to assess the differences in pressure drop. Additionally, the relationship between the cross-sectional area of the flow channel, dynamic pressure, and pressure drop is examined and discussed. The outcomes of this study offer valuable insights and serve as essential reference criteria for optimizing the performance of the receptacle, thereby contributing to advancements in hydrogen refueling technology.

2. Numerical methodology

2.1 Geometry and mesh grids

Fig. 1 illustrates the geometric models of the existing baseline receptacle, its variant, and their internal flow channels. High-pressure hydrogen gas is supplied through the inlet, passes through the receptacle, and enters the vehicle's hydrogen storage tank[10]. The filter section accommodates a filtration mesh to remove contaminants from the supplied hydrogen gas. After filtering, the gas flows through the check valve and is injected into the storage tank. As the flow passes through the filter and check valve section, the significant pressure drop occurs due to the variations of cross-section area and flow direction. Consequently, these two components require particular attention and consideration when redesigning the receptacle.

Fig. 2 shows the mesh grids of the baseline receptacle and receptacle variants generated for numerical simulations. Polyhedral-type meshes are utilized for all grids. Mesh refinement was employed in regions of significant flow variations, such as the throat preceding the filter and the head of the check valve.

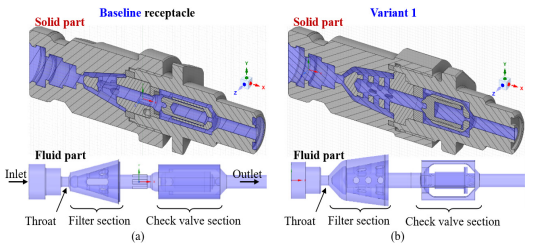

Fig. 1. Geometric models and internal flow paths of the baseline receptacle and a receptacle variant

The total number of cell grids is approximately 2.46 million. Before conducting numerical simulations, a grid dependency analysis was performed, revealing that the pressure variation at the receptacle outlet caused by differences in the mesh was within 0.5%. It shows that the mesh grids used in this study can provide reasonably accurate results.

2.2 Boundary condition

The design condition for the receptacle is set at 70 MPa and -40℃. Therefore, the inlet condition of the receptacle is specified as a pressure inlet at 70 MPa, while the outlet condition is set as a mass flow outlet to calculate the pressure variation. All the information is listed in Table 1.

The throat, located between the inlet and filter section, is where the gas experiences the first flow variation due to a reduction in the path diameter. Therefore, the impact of throat diameter on pressure drop is studied. The baseline receptacle has a throat diameter of 3 mm, while the three variants have throat diameters of 3, 3.8, and 4 mm, respectively.

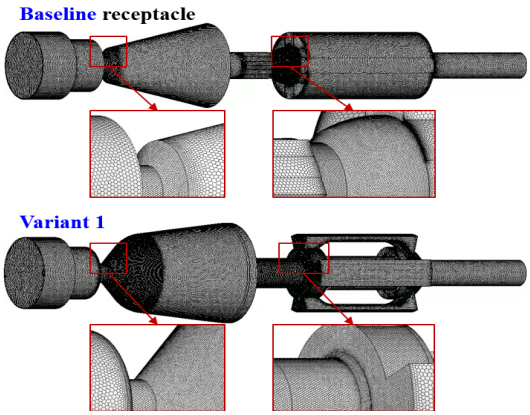

Fig. 2. Mesh grids of the baseline receptacle and a receptacle variant generated for numerical simulations

Table 1. Boundary conditions for the numerical simulation

Parameter/Variable	Value
Inlet pressure inlet [MPa]	70
Outlet mass flow rate [g/s]	52.5
Inlet temperature [K]	233.15
Throat diameter [mm]	3.0, 3.8, 4.0

As shown in Table 2, the density of hydrogen is calculated using the real-gas law. Other properties, such as specific heat capacity, thermal conductivity, and viscosity, are determined using known polynomial models[11].

2.3 Numerical model

The continuity, momentum, and energy equations are summarized in generalized vector forms as follows:

$$\frac{\partial \rho}{\partial t} + \nabla \cdot (\rho \vec{v}) = 0, \tag{1}$$

$$\frac{\partial \rho}{\partial t}(\rho \vec{v}) + \nabla \cdot (\rho \vec{v}\vec{v}) = -\nabla p + \nabla \cdot (\bar{\bar{\tau}}) + \rho \vec{g} + \vec{F}, \tag{2}$$

$$\frac{\partial}{\partial t}(\rho E) + \nabla \cdot (\vec{v}(\rho E + p)) = -\nabla \cdot \left(\sum_j h_j J_j\right) + S_h, \tag{3}$$

where ρ is density, t is time, v is velocity, p is the static pressure, $\bar{\bar{\tau}}$ is the stress tensor, $\rho \vec{g}$ is the gravitational body force, $\vec{F}$ is external body force, E is the total energy, h_i and J_j are the enthalpy and mass flux of species j, and S_h is the source term.

Table 2. Models adopted for calculation of hydrogen properties

Properties of hydrogen	Model
Density [kg/m^3]	Soave-Redlich-Kwong real gas law
Cp [J/(kg·K)]	NASA 9-piecewise polynomial
Thermal conductivity [W/(m·K)]	Polynomial
Viscosity [kg/(m·s)]	Polynomial

To simulate turbulent flow, the above equations (1)-(3) are transformed to Reynolds-averaged Navier-Stokes equations, which form is well known on the basis of *k-ω* turbulent models. All simulations in this study are conducted using the general-purpose computational fluid dynamics code[12]. The shear stress transport k-ω turbulent model is adopted. For spatial discretization of the partial differential equations, the second order upwind scheme is employed.

3. Results and discussion

3.1 Total pressure distribution

Fig. 3 shows the total pressure distribution from the receptacle inlet to the outlet. Both the baseline receptacle and the three variants exhibit the same pressure variation process. The color representing pressure magnitude reveals that pressure drops occur at the throat firstly, where the flow passage diameter abruptly decreases. Furthermore, after passing through the filter section, a pressure reduction is observed. And the pressure further decreases as the fluid continues through the check valve section. After the check valve, there is a final pressure drop before reaching the receptacle outlet.

Fig. 4 provides a detailed depiction of the pressure drop process along a streamline from the receptacle inlet to the outlet. To describe the pressure changes, several specific positions are defined: the inlet, before the filter (BF), after the filter (AF), before the check valve (BC), after the check valve (AC), and the outlet. From Fig. 4, it is seen that the pressure changes from the inlet to BF are relatively minor. However, a sharp pressure drop occurs after BF. Subsequent pressure reductions are observed at AF, BC, and AC. Significant pressure drops are observed between BF and AF, as well as between BC and AC. Therefore, detailed observations and analysis of the filter and the check valve section are necessary.

3.2 Flow inside the filter and check valve sections

Fig. 5 illustrates the streamline and pressure variations in the filter section. It can be observed that there is a pressure gradient starts from the throat. After entering the filter, two recirculation zones, RZ1 and RZ2 are formed. RZ1 exhibits a more pronounced pressure gradient distribution. RZ2 is formed as the

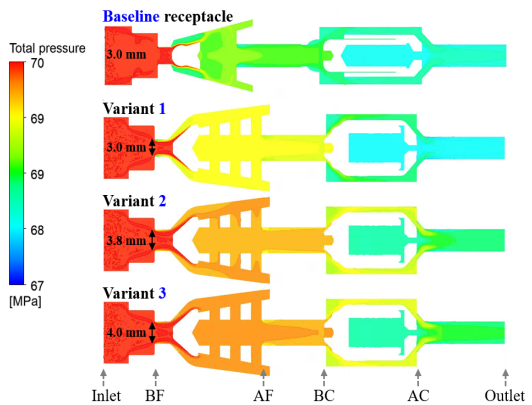

Fig. 3. Total pressure distributions of the baseline receptacle and three variants

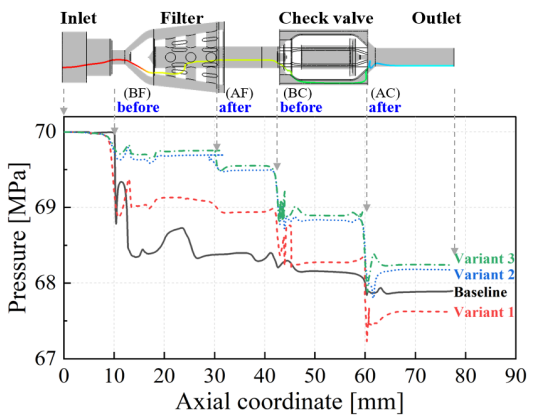

Fig. 4. Pressure variation along the streamline from receptacle inlet to outlet

fluid passes through the filter, but the pressure change in this region is minimal.

Similarly, the streamline and pressure variations in the check valve section can be seen in Fig. 6. The upstream fluid pushes the valve, causing it to open and form a flow passage. Velocity changes occur when the check valve head is impacted, resulting in corresponding pressure gradient distributions. Three variants exhibit more pronounced pressure gradient distributions, as their cross-sectional areas of the check valve section are smaller than the baseline receptacle.

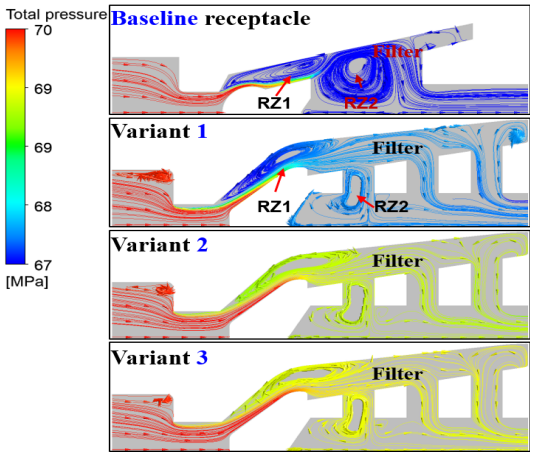

Fig. 5. Streamlines and pressure distribution in the filter section of the baseline receptacle and three receptacles

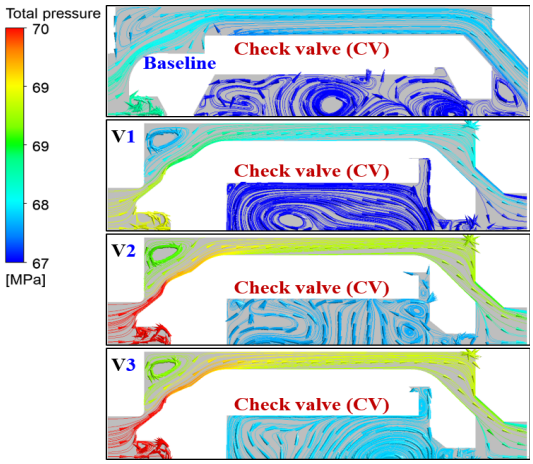

Fig. 6. Streamlines and pressure distribution in the check valve section

3.3 Analysis of pressure drop

For a horizontal pipe, the Darcy-Weisbach equation can be used to calculate the main pressure drop as follows[13]:

$$\Delta P = f \cdot \frac{l}{d} \cdot \frac{\rho v^2}{2}, \tag{4}$$

$$f = \phi\left(Re, \frac{\epsilon}{D}\right), \tag{5}$$

where f is the friction factor, l is the pipe length, d is the diameter, ρ is the fluid density, v represents fluid velocity, Re, the Reynolds number, and ϵ/D is the relative roughness.

For a valve, the additional pressure drop associated with flow is a common minor loss, can be calculated with the following equation[13]:

$$\Delta P = K_L \cdot \frac{1}{2}\rho v^2 \tag{6}$$

where K_L is the loss coefficient.

From equations (4) and (6), it can be seen that if the f and K_L are constant values, the pressure drop will exhibit a direct proportionality to $1/2\rho v^2$, which is the dynamic pressure term of Bernoulli's equation[13]. In this study, the pressure and temperature are the same for all cases, and the geometries of the baseline receptacle and variants are also similar. Therefore, it can be assumed that there is not much difference in f and K_L. Thus, the pressure drop mainly comes from the variation in dynamic pressure.

Fig. 7 illustrates the percentage of dynamic pressure contribution to the total pressure in each receptacle. It can be observed that the percentage of dynamic pressure at BF is relatively high, corresponding to the

significant variations in pressure shown in Fig. 5. Among the three variants, when the throat diameter increases, the decrease in velocity change and the reduction in dynamic pressure result in a lowered pressure drop near the throat. Moreover, it's evident that in the AF position of the receptacle, the dynamic pressure in all three variants is lower compared to the baseline. However, at the check valve, the cross-sectional areas of the variants' BC and AC are smaller than that of the baseline receptacle, resulting in higher pressure drops.

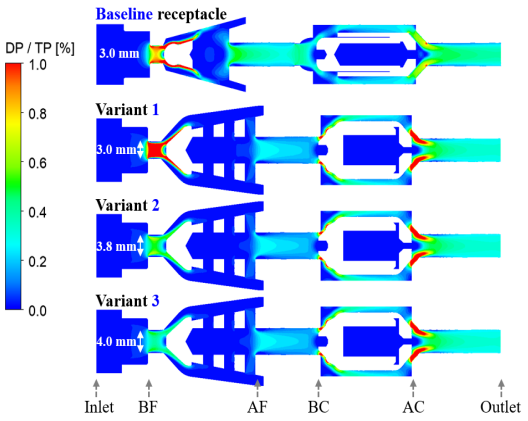

Fig. 7. Distribution of dynamic pressure (DP) as a percentage of total pressure (TP)

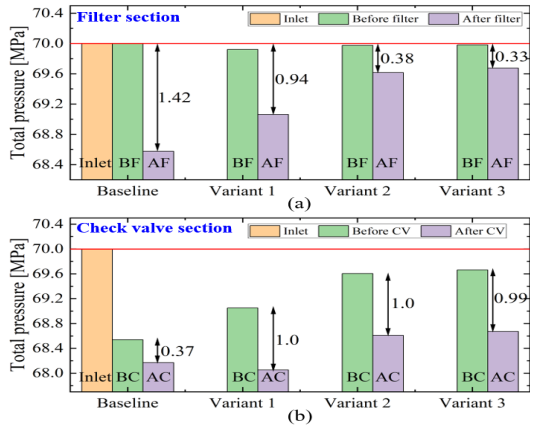

Fig. 8. Pressure variation after fluid through the (a) filter region and (b) the check valve region

Fig. 8 presents the magnitude of pressure drop through the filter and check valve sections. From Fig. 8(a), it can be observed that the pressure drop generated by the variant's filter section is lower than that of the baseline. The filter section of variant 1, which has the same diameter as the baseline, results in a 33.8% lower pressure drop than baseline. Furthermore, as the throat diameter of variants increases, the pressure drop decreases. Modifying the filter section's internal flow channels and increasing the throat diameter can reduce the pressure drop from the initial 1.42 to 0.33 MPa.

In Fig. 8(b), it can be seen that the pressure drop caused by the check valve in the baseline configuration is 0.37 MPa, whereas the pressure drop across the check valves of three variants is approximately 1 MPa. It can be concluded that the baseline check valve performs better. This implies that when improving the variants in the future, special attention should be given to the flow passage at the check valve section.

The variation of the area-averaged total pressure at six positions (inlet, BF, AF, BC, AC, and outlet) in the receptacle is shown in Fig. 9. The baseline receptacle exhibits a significant pressure drop in the filter region and a smaller pressure drop at the check valve region, resulting in a total pressure drop of

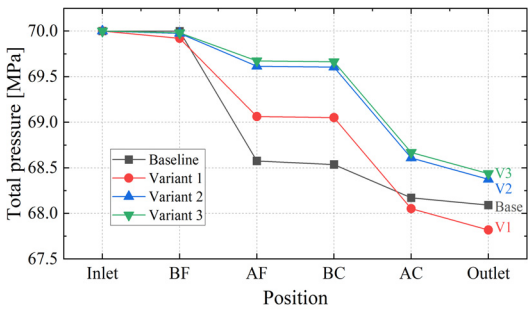

Fig. 9. Area-averaged total pressure at six positions in four receptacles: inlet, before filter (BF), after filter (AF), before check valve (BC), after check valve (AC), and outlet

1.91 MPa from inlet to outlet. In variant 1, the pressure drop in the filter region is slightly smaller than that of the baseline receptacle, but the pressure drop at the check valve region is higher, resulting in a total pressure drop of 2.18 MPa, which is higher than the baseline. In variant 2 and variant 3, the pressure drop in the filter section is further reduced with an increase in throat diameter. As a result, even though the pressure drop in the check valve region remains the same as in variant 1, the total pressure drops in variant 2 and variant 3 are lower than the baseline, which are 1.63 and 1.56 MPa, respectively. Comparing variant 3 with variant 1, by increasing the throat diameter by 1 mm, the total pressure drop is reduced by 0.62 MPa, representing a 28% reduction.

Fig. 10 illustrates the inverse relationship between dynamic pressure and pressure drop with throat diameter. This observation provides validation for the earlier notion that the pressure drop mainly comes from the variation in dynamic pressure. As the throat diameter increases, the cross-sectional area of the flow passage expands, leading to a reduction in fluid velocity.

Additionally, the reduced angle of the flow passage at the filter head results in a gentler change in fluid direction, contributing to the velocity reduction. This can be observed from Fig. 11. In the baseline case, there is a noticeable rapid rise and decline in velocity changes in the radial direction, and a largest peak value. However, in the variants, by adjusting the angle of the flow path at the rear of the throat, the velocity changes become smoother, and with larger throat diameters, the velocity changes become even gentler. These alterations in velocity magnitudes and distributions contribute to reducing pressure losses.

The decrease in flow velocity indicates a gradual diminution of dynamic pressure. As per Equation 6, it can be deduced that pressure drop decreases in line with the reduction in dynamic pressure, consistent with the trend shown in Fig. 10. Based on this trend, further research can focus on optimizing the check valve's flow passage to enhance the receptacle's performance. By carefully designing and adjusting these parameters, it is possible to achieve reduced pressure drop and improved overall efficiency.

4. Conclusion

In this study, the internal flow passage of the receptacle was redesigned based on the baseline receptacle as a reference. The pressure drop between the baseline receptacle and the variants was compared. The findings are as follows:

1) The results demonstrate that the performance of

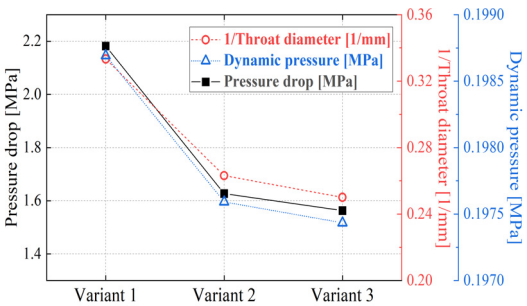

Fig. 10. The relationship between pressure drop, throat diameter and dynamic pressure

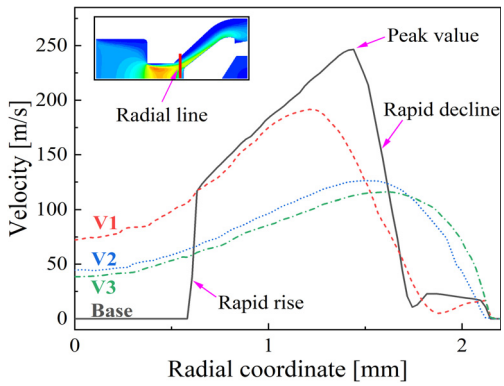

Fig. 11. Velocity distribution along the radial direction near the end of the throat

the variant's filter outperforms the baseline receptacle. However, there is still room for improvement in the check valve compared to the baseline. Under the same throat diameter, the pressure drop in the variant's filter region is 33.8% lower than that of the baseline receptacle.

2) After adjusting the throat diameter, the total pressure drop at the inlet and outlet of the variant is reduced by 28% compared to the baseline receptacle.

3) It was also observed that the pressure drop is directly proportional to the dynamic pressure. When the flow passage area increases, the velocity variation of the fluid becomes uniform, leading to a decrease in both the dynamic pressure and friction generated by the flow, resulting in a reduced pressure drop.

Although this study focused solely on adjusting the throat diameter, the obtained results and the observed trend in pressure drop variations provide valuable insights for future optimization of the internal flow passage in the receptacle.

Acknowledgement

This study was supported by research funding from the Ministry of Trade, Industry, and Energy (MOTIE) and the Korea Evaluation Institute of Industrial Technology (KEIT) in 2023 (Project No. 20015788).

References

1. A. Albatayneh, A. Juaidi, M. Jaradat, and F. Manzano-Agugliaro, “Future of electric and hydrogen cars and trucks: an overview”, Energies, Vol. 16, No. 7, 2023, pp. 3230, doi: https://doi.org/10.3390/en16073230.
2. A. Joshi, “Review of vehicle engine efficiency and emissions”, SAE International journal of advances and current practices in mobility, Vol. 4, No. 5, 2022, pp. 1704-1733, doi: https://doi.org/10.4271/2022-01-0540.
3. L. Fan, Z. Tu, and S. H. Chan, “Recent development of hydrogen and fuel cell technologies: a review”, Energy Reports, Vol. 7, 2021, pp. 8421-8446, doi: https://doi.org/10.1016/j.egyr.2021.08.003.
4. D. Guilbert and G. Vitale, “Hydrogen as a clean and sustainable energy vector for global transition from fossil-based to zero-carbon”, Clean Technologies, Vol. 3, No. 4, 2021, pp. 881-909, doi: https://doi.org/10.3390/cleantechnol3040051.
5. D. Kim, J. S. Lim, and J. Lee, “Current status of standardization for quality control of hydrogen fuel in hydrogen refueling stations for fuel cell electric vehicles”, Journal of Hydrogen and New Energy, Vol. 33, No. 4, 2022, pp. 284-292, doi: https://doi.org/10.7316/KHNES.2022.33.4.284.
6. J. Ye, Z. Zhao, J. Cui, Z. Hua, W. Peng, and P. Jiang, “Transient flow behaviors of the check valve with different spool-head angle in high-pressure hydrogen storage systems”, Journal of Energy Storage, Vol. 46. 2022, pp. 103761, doi: https://doi.org/10.1016/j.est.2021.103761.
7. J. Ye, J. Cui, Z. Hua, J. Xie, W. Peng, and W. Wang, “Study on the high-pressure hydrogen gas flow characteristics of the needle valve with different spool shapes”, International Journal of Hydrogen Energy, Vol. 48, No. 30, 2023, pp. 11370-11381, doi: https://doi.org/10.1016/j.ijhydene.2022.04.073.
8. J. Lee, S. Han, H. Kim, G. Kim, and J. Kim, “Numerical study for flow noise reduction of receptacle for hydrogen charging in FCEV”, 2018 KSAE Annual Conference, Vol. 2018, 2018, pp. 186. Retrieved from https://www.dbpia.co.kr/journal/articleDetail?nodeId=NODE07593039&nodeId=NODE07593039&medaTypeCode=185005&language=ko_KR&hasTopBanner=true.
9. J. H. Choi, G. H. Kim, J. K. Kim, Y. K. Kim, and H. K. Suh, “Analysis of flow performance according to actuator geometry of receptacle for hydrogen charging system with filter applied”, Journal of Hydrogen and New Energy, Vol. 34, No. 1, 2023, pp. 17-25, doi: https://doi.org/10.7316/KHNES.2023.34.1.17.
10. J. Q. Li, H. Xu, J. C. Li, and J. T. Kwon, “A theoretical study on the compressibility factor of hydrogen gas in the high pressure tank”, Journal of Hydrogen and New Energy, Vol. 34, No. 2, 2023, pp. 162-168, doi: https://doi.org/10.7316/JHNE.2023.34.2.162.
11. ANSYS, “ANSYS Fluent theory guide: release 2021 R2”, ANSYS, 2021. Retrieved from https://dl.cfdexperts.net/cfd_resources/Ansys_Documentation/Fluent/Ansys_Fluent_Theory_Guide.pdf.
12. ANSYS, " ANSYS Fluent user guide : realese 13.0", ANSYS, 2010. Retrived from https://www.fluid.tuwien.ac.at/322057?action=AttachFile&do=get&target=flu_ug.pdf.
13. B. R. Munson, T. H. Okiishi, W. W. Huebsch, and A. P. Rothmayer, “Fundamentals of fluid mechanics”, 7th ed., John Wiley & Sons, USA, 2013.